Detection in Ambient Backscatter Communication System with Multi-Antenna Tag-Reader Pair with Correlated Ambient Source Signal

Anuranjan Jha, Adarsh Patel
School of Computing and Electrical Engineering (SCEE), Indian Institute of Technology Mandi, H.P. India
Email: d20008@students.iitmandi.ac.in, adarsh@iitmandi.ac.in

***Abstract*—This paper considers a multiple-input multiple-output (MIMO) setup between tag and reader in AmBC system, where the tag communicates with the reader in the presence of a correlated RF source signal. A maximum signal-to-interference-plus-noise ratio (SINR) optimal combining detector (MSOCD) is proposed to detect the tag's embedded information by maximizing the SINR at the reader. Closed-form expressions for the probability of false alarm and the probability of detection are derived to characterize the performance of the proposed MSOCD. In simulation, receiver operating characteristic (ROC) analysis demonstrates that the MSOCD achieves superior detection performance compared to state-of-the-art (SOTA) detectors. The theoretical findings are further validated through simulations, with ROC plots confirming the accuracy of the analytical derivations.**

***Index Terms*—Ambient backscatter communication (AmBC), correlated signal, optimal combiner.**

I. Introduction

With growing demands for energy-efficient, sustainable IoT connectivity, Ambient Backscatter Communication (AmBC) has emerged as a promising ultra-low-power technology for Green IoT in next-generation 6G networks [1]. It enables communication between a passive tag and a reader by modulating and reflecting existing RF signals through adjustment of the tag's antenna load impedance. The tag encodes information onto the incident RF signal, generating a backscattered signal with modified amplitude or phase. By leveraging ambient RF sources like TV towers, cellular base stations, or Wi-Fi access points, AmBC eliminates the need for active RF components at the tag, aligning with Green IoT principles of low energy consumption and minimal electronic waste [2]. AmBC supports scalable and sustainable IoT applications, including smart homes, IoT networks, healthcare monitoring, and supply chain management [3], [4]. However, the reliance on ambient RF signals introduces a fundamental challenge in detecting the weak backscattered signal at the reader. This detection problem is particularly challenging in the presence of strong direct-link interference from the RF source and under fading-dominated channels and low SINR conditions [5].

In the AmBC system, general research work has utilized an energy detector (ED) due to its simplicity, as seen in [6]–[8]. Variants of the ED framework, including maximum a posteriori (MAP)-based detectors [9], [10] and maximum likelihood (ML)-based designs [11], have been shown to be equivalent to the conventional ED. In the multi-antenna case in AmBC, research has explored advanced detectors for performance gains. The MAP-based optimal detector for uncorrelated RF sources presented in [12] and the average power detection strategy in [13] were used for detecting the tag signals. Eigenvalue-centric approaches, such as the maximum eigenvalue detector (M-EVD) [14] and beamforming-based ED [15], exploit spatial diversity to enhance detection. In [16], a statistical covariance-based detector was proposed, which analyzes two covariance statistics derived from the sample covariance matrices to determine the presence or absence of the tag signal. Moreover, adaptive MAP architectures [17] extend this approach to M-ary frequency-shift keying modulation, and ML-based ratio detectors [18] have emerged to address modulation-specific constraints. Notably, the improved energy detector (IED) introduced in [10], [19] leverages a p-norm framework to outperform conventional ED under correlated fading environments.

Several recent works on multi-antenna systems in AmBC have been studied. Optimal detectors based on the MAP criterion are developed in [20]. In contrast, machine-learning-based methods have also been considered, with [21] employing support vector machines (SVM) and random forests (RF), and [22] adopting k-nearest neighbors (kNN). These contributions demonstrate significant progress for multiple antennas at the reader in AmBC. There is limited work on MIMO-based AmBC systems. For example, the work in [23] utilizes average energy for detection, while [2], [24] investigates ML-based detectors. This highlights an important direction for advancing MIMO detection techniques in AmBC systems.

The works on AmBC in [6]–[25] primarily consider scenarios in which the RF source signals are assumed to be uncorrelated, thereby neglecting the potential correlation that exist among them [26]–[28]. However, in practical wireless communication environments, such as cellular networks and Wi-Fi systems, RF source signals often exhibit correlation due to shared interference, overlapping transmissions, and common propagation conditions [27]–[29]. Such correlations can significantly affect the received signal structure at backscatter tags and readers, altering detection performance and challenging traditional detection schemes that assume independent RF source signals. Hence, the present work develops a detection framework that explicitly accounts for RF source

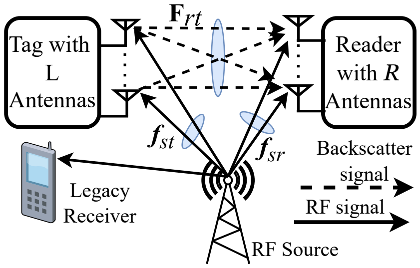

Fig. 1: AmBC system comprises a legacy receiver, tag with L antennas, a reader with R antennas, and a single-antenna RF source.

signal correlation, providing accurate modeling and improved detection performance in a realistic AmBC system. The key contributions of the proposed work are summarized as follows:

- A detector (MSOCD) is developed for the MIMO AmBC system with correlated RF source signals, where the MSOCD optimally combines the received vector to maximize the SINR at the reader.
- Closed-form expressions for the probability of false alarm and detection are obtained to analyze the performance of the proposed detector.
- ROC analysis shows that the proposed detector consistently outperforms state-of-the-art (SOTA) detectors, and simulations validate the analytical derivations, confirming the superior detection performance of the MSOCD.

Section II introduces the system model of the MIMO AmBC framework between tag and reader with correlated RF source signals. Section III present the formulation of MSOCD, and Section IV present performance characterization of MSOCD. Section V provides simulation results, and Section VI concludes the paper and discusses potential future research directions. Notation used in this paper: vectors by lowercase boldface letters, and matrices by uppercase boldface letters. The transpose, Hermitian, and inverse of a matrix $\mathbf{X}$ are represented as $\mathbf{X}^T$, $\mathbf{X}^H$, and $\mathbf{X}^{-1}$, respectively, $\mathbf{I}_K$ is $K \times K$ identity matrix. The expectation and probability are denoted by $\mathbb{E}[\cdot]$ and $\Pr(\cdot)$, respectively. The set of complex numbers as $\mathbb{C}$, and $x \sim \mathcal{CN}(\mu, \sigma^2)$ represents a circularly symmetric complex Gaussian random variable with mean μ and variance σ^2. A chi-square random variable with k degrees of freedom is denoted by χ^2_k, and $Q_{\chi^2_k}(\cdot)$ denotes right-tail probability of the chi-square distribution.

II. MIMO AmBC System with Multi-Antenna Tag and Reader

Consider the MIMO AmBC system shown in Fig. 1, where the RF source uses a single antenna, the tag (backscatter transmitter) is equipped with L antennas, and the reader (backscatter receiver) employs R antennas. The RF source transmits a symbol u_k intended for its legacy user at the k-th time instant. The received signal vector at the tag, denoted by $\mathbf{q}_k \in \mathbb{C}^{L\times 1}$ for the k-th sample, is given by

$$\mathbf{q}_k = \mathbf{f}_{st}\, u_k, \tag{1}$$

where $\mathbf{f}_{st} = [f_{st_1} \dots f_{st_L}]^T \in \mathbb{C}^{L\times 1}$ characterizes the flat Rayleigh fading channel between the RF source and the L tag antennas. To convey its binary information bits $\mathrm{b} \in \{0, 1\}$, tag modulates the impinging signal by altering the impedance across the tag's load. Let α denote the reflection efficiency of the tag. The resulting backscattered signal $\mathbf{q}_{\mathrm{b}_k} \in \mathbb{C}^{L\times 1}$ can be expressed as

$$\mathbf{q}_{\mathrm{b}_k} = \alpha\, \mathbf{q}_k\, \mathrm{b}. \tag{2}$$

Let $\mathbf{f}_{sr} = [f_{sr_1} \dots f_{sr_R}]^T \in \mathbb{C}^{R\times 1}$ denote the channel vector between the RF source and the R antennas at the reader. Similarly, let $\mathbf{F}_{rt} \in \mathbb{C}^{R\times L}$ denote the channel matrix from the tag to the reader, where each element is given by $[\mathbf{F}_{rt}]_{r,l} = f_{rt_{r,l}}$ for $r = 1 \cdots R$ and $l = 1 \cdots L$. The signal received at the reader for $k-$th RF source sample, $\mathbf{z}_k \in \mathbb{C}^{R\times 1}$, can be expressed as

$$\mathbf{z}_k = \mathbf{f}_{sr} u_k + \mathbf{F}_{rt}\, \mathbf{q}_{\mathrm{b}_k} + \mathbf{n}_k \tag{3}$$

$$= \mathbf{f}_{sr} u_k + \mathbf{F}_{rt}\, \alpha\, \mathbf{f}_{st}\, u_k\, \mathrm{b} + \mathbf{n}_k, \tag{4}$$

where $\mathbf{n}_k \in \mathbb{C}^{R\times 1}$ is the additive white Gaussian noise (AWGN) vector with distribution $\mathcal{CN}(\mathbf{0}, \sigma^2\mathbf{I}_R)$. Equation (4) is obtained by substituting (2) into (3). Stacking K source symbols, the composite received signal at the reader can be written as $\mathbf{z} = [\mathbf{z}_1^T \dots \mathbf{z}_k^T \dots \mathbf{z}_K^T]^T \in \mathbb{C}^{RK\times 1}$. This yields the compact form as

$$\mathbf{z} = \mathbf{F}_{sr}\mathbf{u} + \mathbf{F}_{str}\mathbf{u}\,\mathrm{b} + \mathbf{n}, \tag{5}$$

where, $\mathbf{F}_{sr} = \mathbf{I}_K \otimes \mathbf{f}_{sr} \in \mathbb{C}^{RK\times K}$, $\mathbf{F}_{str} = \alpha(\mathbf{I}_K \otimes \mathbf{F}_{rt}\mathbf{f}_{st}) \in \mathbb{C}^{RK\times K}$, $\mathbf{u} = [u_1 \dots u_K]^T \in \mathbb{C}^{K\times 1}$ is the RF source signal vector, and $\mathbf{n} = [\mathbf{n}_1^T \dots \mathbf{n}_K^T]^T \in \mathbb{C}^{RK\times 1}$ is the stacked AWGN vector with distribution $\mathcal{CN}(\mathbf{0}, \sigma^2\mathbf{I}_{RK})$. Let RF source signal vector $\mathbf{u}$ follow multivariate complex Gaussian distribution with zero mean and covariance $\mathbf{C}_\mathbf{u} \in \mathbb{C}^{K\times K}$, i.e., $\mathbf{u} \sim \mathcal{CN}(\mathbf{0}, \mathbf{C}_\mathbf{u})$ [30]. This work assumes the channels and covariance matrix to be known. However these can be estimated at the receiver and the effect of the estimation error is illustrated in the simulation section.

III. Maximum-SINR Optimal Combining Detector (MSOCD)

This section develops the MSOCD for the MIMO AmBC system described in Section II. The aim is to design a combining vector at the reader that maximizes the SINR defined in (6). Consider a linear combining vector $\mathbf{w} \in \mathbb{C}^{RK\times 1}$ applied to $\mathbf{z}$. The combined signal at the reader is obtained as

$$\mathbf{w}^H\mathbf{z} = \underbrace{\mathbf{w}^H\mathbf{F}_{sr}\mathbf{u}}_{\text{Interference}} + \underbrace{\mathbf{w}^H\mathbf{F}_{str}\mathbf{u}\,\mathrm{b}}_{\text{Tag signal}} + \underbrace{\mathbf{w}^H\mathbf{n}}_{\text{Noise}}. \tag{6}$$

The signal-to-interference-plus-noise ratio (SINR) at the output of the linear combiner $\mathbf{w}$ is defined as the ratio of the average power of the tag signal to the average power of the interference and noise components in (6), i.e.,

$$F_{\text{SINR}}(\mathbf{w}) = \frac{\mathbb{E}\left[\left|\mathbf{w}^H\mathbf{F}_{str}\mathbf{u}\,\mathrm{b}\right|^2\right]}{\mathbb{E}\left[\left|\mathbf{w}^H\mathbf{F}_{sr}\mathbf{u}\right|^2\right]+\mathbb{E}\left[\left|\mathbf{w}^H\mathbf{n}\right|^2\right]} \tag{7}$$

$$= \frac{\mathbb{E}[\mathrm{b}^2]\,\mathbf{w}^H\mathbf{F}_{str}\mathbf{C}_{\mathbf{u}}\mathbf{F}_{str}^H\mathbf{w}}{\mathbf{w}^H\mathbf{F}_{sr}\mathbf{C}_{\mathbf{u}}\mathbf{F}_{sr}^H\mathbf{w}+\sigma^2\mathbf{w}^H\mathbf{w}}, \tag{8}$$

where $\mathbf{C}_{\mathbf{u}} = \mathbb{E}\{\mathbf{u}\mathbf{u}^H\}$ is the covariance matrix of the RF source signal in (8). Define the matrices $\mathbf{R}_{str} = 0.5\,\mathbf{F}_{str}\mathbf{C}_{\mathbf{u}}\mathbf{F}_{str}^H$, and $\mathbf{R}_{sr} = \mathbf{F}_{sr}\mathbf{C}_{\mathbf{u}}\mathbf{F}_{sr}^H + \sigma^2\mathbf{I}_{RK}$. The factor $\mathbb{E}[\mathrm{b}^2] = 0.5$ arises since the tag bit $\mathrm{b} \in \{0,1\}$ is equally likely. Upon substituting $\mathbf{R}_{str}$ and $\mathbf{R}_{sr}$ in the SINR in (8) can be rewritten as

$$F_{\text{SINR}}(\mathbf{w}) = \frac{\mathbf{w}^H\mathbf{R}_{str}\mathbf{w}}{\mathbf{w}^H\mathbf{R}_{sr}\mathbf{w}}. \tag{9}$$

The optimal combining vector $\mathbf{w}$, which maximizes the SINR in (9) at the reader, is obtained by solving the following optimization problem:

$$\max_{\mathbf{w}} \quad F_{\text{SINR}}(\mathbf{w}), \qquad \text{s.t.} \quad \|\mathbf{w}\| \le 1. \tag{10}$$

The combining vector $\mathbf{w}$ that solves the optimization problem (10) admits an explicit solution. Upon maximizing the cost function in (10), it is determined by the eigenvector associated with the largest eigenvalue of the matrix $\mathbf{\Psi} = \mathbf{R}_{sr}^{-1}\mathbf{R}_{str} \in \mathbb{C}^{RK\times RK}$. In this setting, the objective in (9) reaches its maximum when the optimal combining vector $\mathbf{w}^\star$ is chosen as the eigenvector to the largest eigenvalue of $\mathbf{\Psi}$. Consequently, the test for MSOCD for the considered MIMO AmBC scenario with correlated RF source signals is formulated as

$$\mathcal{T}_{\text{MSOCD}}(\mathbf{z}) = \mathbf{w}^{\star H}\mathbf{z} \underset{\hat{\mathrm{b}}=0}{\overset{\hat{\mathrm{b}}=1}{\gtrless}} \gamma, \tag{11}$$

where $\hat{\mathrm{b}}$ is the detected tag bit and γ is the detection threshold. The matrices $\mathbf{R}_{sr}$ and $\mathbf{R}_{str}$ in (9) depend on channel matrices and the correlated RF source covariance $\mathbf{C}_{\mathbf{u}}$. The proposed MSOCD exploits this correlation to obtain $\mathbf{w}^\star$ in (11), maximizing SINR and is SINR-optimal while accounting for correlated interference that SOTA detectors overlook. For independent RF source signals, i.e., $\mathbf{C}_{\mathbf{u}} = P_{\mathbf{u}}\mathbf{I}_K$, the matrix $\mathbf{\Psi}$ simplifies to $\mathbf{\Psi} = \frac{1}{2}\left(\mathbf{F}_{sr}\mathbf{F}_{sr}^H + \frac{\sigma^2}{P_{\mathbf{u}}}\mathbf{I}_{RK}\right)^{-1}\mathbf{F}_{str}\mathbf{F}_{str}^H$ without a change in the remaining analysis. The next section analyzes the MSOCD's performance to characterize its detection.

IV. Performance Analysis of MSOCD

The performance of the MSOCD in (11) is evaluated by deducing the probability density functions (PDFs) of the test statistic $\mathcal{T}_{\text{MSOCD}}(\mathbf{z})$ in (11) for hypotheses $\mathcal{H}_0$ and $\mathcal{H}_1$. Let $\mathcal{H}_0$ correspond to $\mathrm{b} = 0$, and $\mathcal{H}_1$ correspond to $\mathrm{b} = 1$. Under hypothesis $\mathcal{H}_i$, the test statistic $\mathcal{T}_{\text{MSOCD}}(\mathbf{z})$ follows a complex Gaussian distribution with zero mean and variance, σ_i^2 as the test statistic is a linear combination of the complex Gaussian vector $\mathbf{z}$. For hypothesis $\mathcal{H}_i$, the variance σ_i^2 is given by

$$\sigma_i^2 = \operatorname{var}\big(\mathcal{T}_{\text{MSOCD}}(\mathbf{z})\,\big|\,\mathcal{H}_i\big) = \mathbf{w}^{\star H}\,\mathbf{R}_{\mathbf{z}|i}\,\mathbf{w}^\star, \tag{12}$$

with $\mathbf{R}_{\mathbf{z}|i}$ denoting the covariance matrix of the received signal $\mathbf{z}$ in (5) under $\mathcal{H}_i$. The received signal corresponding to the hypothesis $\mathcal{H}_i$ is expressed as

$$\mathcal{H}_i: \quad \mathbf{z} = \mathbf{F}_i\mathbf{u} + \mathbf{n}, \tag{13}$$

where $\mathbf{F}_i$, for $i \in \{0,1\}$, is defined as $\mathbf{F}_0 = \mathbf{F}_{sr}$ and $\mathbf{F}_1 = \mathbf{F}_{sr} + \mathbf{F}_{str}$. The received-signal covariance matrix $\mathbf{R}_{\mathbf{z}|i} = \mathbb{E}[\mathbf{z}\mathbf{z}^H|\mathcal{H}_i]$ of $\mathbf{z}$ in (13) under hypothesis $\mathcal{H}_i$ is obtained as

$$\mathbf{R}_{\mathbf{z}|i} = \mathbf{F}_i\mathbf{C}_{\mathbf{u}}\mathbf{F}_i^H + \sigma^2\mathbf{I}_{RK}. \tag{14}$$

Since $\mathcal{T}_{\text{MSOCD}}(\mathbf{z}) \sim \mathcal{CN}(0,\sigma_i^2)$, the normalized test statistic under hypothesis $\mathcal{H}_i$, for $i \in \{0,1\}$, follows a chi-square distribution with two degrees of freedom, i.e., χ_2^2 defined as

$$\mathcal{H}_i: \quad \frac{1}{\sigma_i^2}\left|\mathcal{T}_{\text{MSOCD}}(\mathbf{z})\right|^2 \sim \chi_2^2, \qquad i \in \{0,1\}. \tag{15}$$

The following subsections present the probability of false alarm and probability of detection.

A. Probability of False Alarm (P_{FA})

The probability of false alarm is defined as detecting the tag symbol $\mathrm{b} = 1$ when the actual transmitted symbol was $\mathrm{b} = 0$. As described in (16) and further simplified as

$$P_{FA} = \Pr\{\mathcal{T}_{\text{MSOCD}}(\mathbf{z}) > \gamma \,|\, \mathcal{H}_0\} \tag{16}$$

$$= \Pr\left\{\frac{1}{\sigma_0^2}\left|\mathcal{T}_{\text{MSOCD}}(\mathbf{z})\right|^2 > \frac{\gamma^2}{\sigma_0^2}\right\} \tag{17}$$

$$= Q_{\chi_2^2}\left(\frac{\gamma^2}{\sigma_0^2}\right), \tag{18}$$

where in (17), the test statistic is normalized with respect to the variance under $\mathcal{H}_0$, and (18) follows from the tail probability of a chi-squared distribution with two degrees of freedom, as in (15) under the null hypothesis $\mathcal{H}_0$.

B. Probability of Detection (P_D)

The probability of detection (P_D) is defined as detecting the tag symbol $\mathrm{b} = 1$ when the actual transmitted symbol was $\mathrm{b} = 1$. The expression for P_D can be obtained in a manner similar to the proof of P_{FA} in (16). An outline is presented below:

$$P_D = \Pr\{\mathcal{T}_{\text{MSOCD}}(\mathbf{z}) > \gamma \,|\, \mathcal{H}_1\}$$

$$= \Pr\left\{\frac{1}{\sigma_1^2}\left|\mathcal{T}_{\text{MSOCD}}(\mathbf{z})\right|^2 > \frac{\gamma^2}{\sigma_1^2}\right\}, \tag{19}$$

$$= Q_{\chi_2^2}\left(\frac{\gamma^2}{\sigma_1^2}\right). \tag{20}$$

In (19), the test statistic is normalized by the variance under $\mathcal{H}_1$, and (20) is obtained from the tail probability of a chi-squared distribution with two degrees of freedom, as given in (15) under the alternative hypothesis $\mathcal{H}_1$. The next section presents simulation results to validate the analysis and demonstrate the performance of MSOCD.

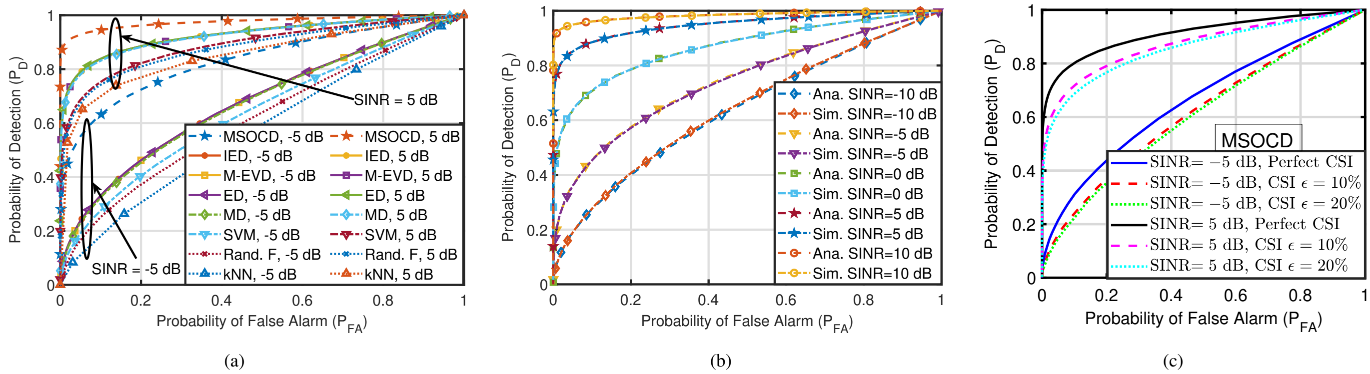

Fig. 2: ROC curves of the proposed MSOCD in (11) at number of tag antenna $L = 3$ and $P_{\mathbf{u}} = 0.01$ W: (a) Performance comparison with SOTA detectors, including IED [19], M-EVD [14], ED [7], MD [19], SVM, random forest (Rand. F) [21], and kNN [22], at SINR $\in \{-5, 5\}$ dB with $R = 3$, and $K = 3$. (b) Validation of analytical (Ana.) expressions for P_{FA} in (18) and P_D in (20) against simulations (Sim.) at SINR $\in \{-10, -5, 0, 5, 10\}$ dB with $K = 2$, and $R = 3$. (c) Performance under imperfect CSI with estimation error $\epsilon \in \{0\%, 10\%, 20\%\}$ at SINR $\in \{-5, 5\}$ dB with $K = 2$ and $R = 3$.

V. Simulation Results

Consider the MIMO AmBC system in (5), with the entries of the true channel coefficient matrices $\mathbf{F}_{sr}$ and $\mathbf{F}_{str}$ are drawn from a standard complex Gaussian distribution. The error $\mathbf{E}$ in the true channel $\mathbf{H} \in \{\mathbf{F}_{sr}, \mathbf{F}_{str}\}$ be modeled as the estimated channel $\hat{\mathbf{H}} = \mathbf{H} + \mathbf{E}$, where the elements of $\mathbf{E}$ are i.i.d. $\mathcal{CN}(0, \epsilon\sigma_h^2)$ with $\epsilon \in \{0\%, 10\%, 20\%\}$. The correlated RF source signal vector $\mathbf{u}$, relevant to the applications discussed in [27]–[29], follows a complex Gaussian distribution with zero mean and covariance matrix $\mathbf{C_u}$, i.e., $\mathbf{u} \sim \mathcal{CN}(\mathbf{0}, \mathbf{C_u})$. To capture general correlation structures without restricting to a specific parametric model, the covariance matrix $\mathbf{C_u}$ is generated via eigenvalue decomposition $\mathbf{C_u} = \mathbf{V}\boldsymbol{\Lambda}\mathbf{V}^H$, where $\mathbf{V}$ is a unitary matrix and $\boldsymbol{\Lambda}$ is a diagonal matrix with its main diagonal entries uniformly spaced between two positive numbers, normalized by the power $P_{\mathbf{u}}$. The transmission rate of the RF source is set to thrice that of the tag signal, i.e., $K = 3$. The backscatter tag symbol $\mathrm{b} \in \{0, 1\}$ is modeled as a binary random variable with equal probability, with backscatter efficiency α fixed to unity [10], [19]. The additive noise vector $\mathbf{n}$ is assumed to be complex Gaussian with zero mean and covariance matrix $\mathbf{I}_{RK}$. The proposed MSOCD statistic $\mathcal{T}_{\text{MSOCD}}(\mathbf{z})$ in (11) is compared against allied detectors, where the M-EVD exhibits a comparable implementation complexity.

Fig. 2a compares the ROC performance of the proposed MSOCD with IED [19], M-EVD [14], ED [7], and MD [19] in AmBC systems with the number of RF source samples $K = 3$, the number of reader antennas $R = 2$, and the number of tag antennas $L = 3$, at different SINR levels. The results show that the MSOCD consistently achieves superior ROC performance, with a significant margin over the competing detectors, across all considered SINR values SINR $\in \{-5, 5\}$ dB. The MSOCD has computational complexity $\mathcal{O}((RK)^3)$ same as M-EVD, whereas other detectors such as IED, ED, and MD have $\mathcal{O}(RK)$ complexity order but inferior performance, as it ignores covariance information. The learning-based approaches such as kNN [22], SVM, and Random Forest [21] have been compared with MSOCD. These methods classify signals by similarity (kNN), by learning optimal decision boundaries (SVM), and by leveraging ensembles of decision trees (Random Forest). However, these machine learning approaches require supervised training with tag bits $\mathrm{b} \in \{0, 1\}$ for each SINR level, typically using 10^5 labeled samples, which significantly increases computational overhead compared to the MSOCD. Fig. 2b shows the ROC equivalence between the simulated results and the analytical probabilities derived in (18) and (20) for the MSOCD at different SINR values $\{-10, -5, 0, 5, 10\}$ dB. Fig. 2c shows the robustness of MSOCD under imperfect CSI with different estimation error $\epsilon \in \{0\%, 10\%, 20\%\}$, where $\epsilon = 0\%$ denotes perfect CSI. The results indicate only gradual performance degradation with increasing estimation error.

Fig. 3a illustrates the ROC performance of the MSOCD for different numbers of receive antennas, $R \in \{2, 3, 5\}$, at the reader. Fig. 3b compares the ROC performance for different numbers of RF source signals, $K \in \{2, 4, 8\}$. An improvement in detection performance is observed as K increases, since a larger number of RF source samples provides additional signal diversity at the reader. Moreover, increasing the number of reader antennas R further enhances the spatial combining capability, leading to higher SINR at the detector output. Fig. 3c presents the ROC performance of the MSOCD under varying RF source power levels, $P_{\mathbf{u}} \in \{0.001, 0.2, 1\}$ W. Improved detection performance is observed at lower values of $P_{\mathbf{u}}$, since reducing the RF source power increases the effective SINR in (8) by enhancing the relative strength of the backscattered tag signal and improving the separability between $\mathcal{H}_0$ and $\mathcal{H}_1$. ROC curves in Figs. 3b and 3c are truncated; the underlying trends are unaffected.

VI. Conclusions and Future Work

This paper presented the design and analysis of MSOCD for MIMO-based AmBC system in the presence of correlated ambient RF source signals. The ROC comparisons in the simulation section demonstrated that MSOCD outperformed SOTA detectors, including the IED, ED, M-EVD, and MD,

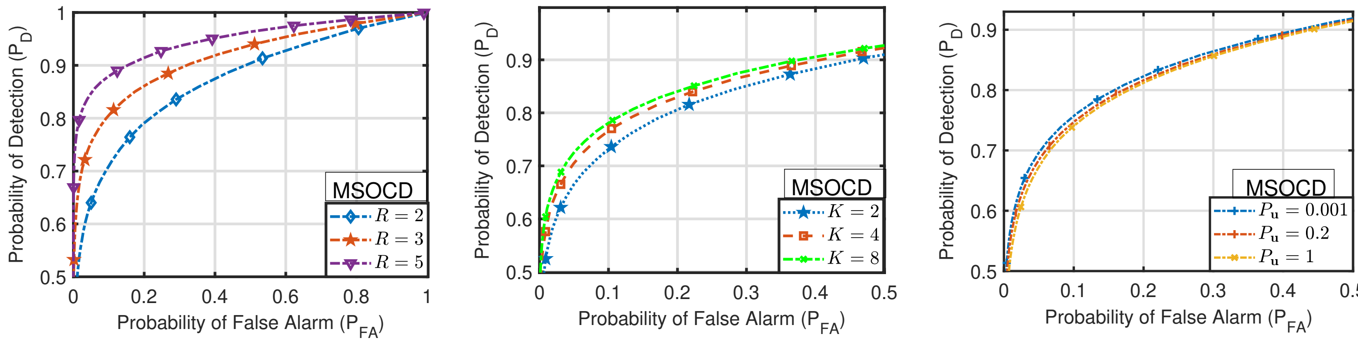

(a) (b) (c)

Fig. 3: ROC performance of the proposed MSOCD in (11) at $L = 3$ and $\mathrm{SINR} = 0$ dB: (a) performance for different numbers of reader antennas, $R \in \{2, 3, 5\}$; (b) performance for different numbers of RF source samples, $K \in \{2, 4, 8\}$ with $R = 3$ and $P_{\mathbf{u}} = 0.01$ W; and (c) performance under different RF source signal power levels, $P_{\mathbf{u}} \in \{0.001, 0.2, 1\}$ W with $R = 3$ and $K = 2$.

as well as machine learning-based approaches such as SVM, random forest, and kNN. In addition, closed-form expressions for P_{FA} and P_D were derived within the considered AmBC framework. The results demonstrated a close match between the analytical derivations and simulation outcomes.

References

[1] N. V. Huynh, D. T. Hoang, X. Lu, D. Niyato, P. Wang, and D. I. Kim, "Ambient Backscatter Communications: A Contemporary Survey," *IEEE Commun. Surv. Tutor.*, vol. 20, no. 4, pp. 2889–2922, 2018.

[2] D. Cheng, F. Wu, C. Zhang, W. Fan, and Y. Liu, "Design and Performance of Passive Virtual MIMO in Ambient Backscatter Communication," *IEEE Wireless Commun. Lett.*, vol. 13, no. 3, pp. 612–616, 2024.

[3] J. Xin and S. Xu, "Cellular Backscatter Communication: Ambient IoT Technology," in *IEEE Int. Symp. Broadcast. Multimedia Syst.*, pp. 1–6, 2024.

[4] Y. Yang, Y. Feng, W. Gong, and Y. Yang, "Efficient LTE Backscatter with Uncontrolled Ambient Traffic," in *IEEE INFOCOM*, pp. 1781–1790, 2024.

[5] F. Rezaei, C. Tellambura, and S. Herath, "Large-Scale Wireless-Powered Networks with Backscatter Communications—A Comprehensive Survey," *IEEE Open J. Commun. Soc.*, vol. 1, pp. 1100–1130, 2020.

[6] G. Wang, F. Gao, R. Fan, and C. Tellambura, "Ambient Backscatter Communication Systems: Detection and Performance Analysis," *IEEE Trans. Commun.*, vol. 64, no. 11, pp. 4836–4846, 2016.

[7] J. K. Devineni and H. S. Dhillon, "Ambient Backscatter Systems: Exact Average Bit Error Rate under Fading Channels," *IEEE Trans. Green Commun. Netw.*, vol. 3, no. 1, pp. 11–25, 2019.

[8] Q. Tao, C. Zhong, X. Chen, Q. Wu, and Z. Zhang, "Ambient Backscatter Communication Systems with Multi-Antenna Reader," in *Asia-Pac. Conf. Commun.*, pp. 245–250, 2018.

[9] J. Qian, F. Gao, G. Wang, S. Jin, and H. Zhu, "Noncoherent Detections for Ambient Backscatter System," *IEEE Trans. Wireless Commun.*, vol. 16, no. 3, pp. 1412–1422, 2017.

[10] Y. Chen and W. Feng, "Novel Signal Detectors for Ambient Backscatter Communications in Internet of Things Applications," *IEEE Internet Things J.*, vol. 11, no. 3, pp. 5388–5400, 2024.

[11] J. Qian, F. Gao, G. Wang, S. Jin, and H. Zhu, "Semi-Coherent Detection and Performance Analysis for Ambient Backscatter System," *IEEE Trans. Commun.*, vol. 65, no. 12, pp. 5266–5279, 2017.

[12] Q. Tao, C. Zhong, X. Chen, H. Lin, and Z. Zhang, "Optimal Detection for Ambient Backscatter Communication Systems with Multiantenna Reader under Complex Gaussian Illuminator," *IEEE Internet Things J.*, vol. 7, no. 12, pp. 11371–11383, 2020.

[13] Y. Liu, Z. Zhong, G. Wang, and D. Hu, "Uplink Detection and BER Performance for Wireless Communication Systems with Ambient Backscatter and Multiple Receiving Antennas," in *Int. Conf. Commun. Netw. China*, pp. 79–84, 2015.

[14] Q. Tao, C. Zhong, X. Chen, and Z. Zhang, "Maximum-Eigenvalue Detector for Multi-Antenna Ambient Backscatter Communication Systems," in *IEEE Int. Conf. Commun.*, pp. 1–5, 2019.

[15] H. Guo, Q. Zhang, S. Xiao, and Y.-C. Liang, "Exploiting Multiple Antennas for Cognitive Ambient Backscatter Communication," *IEEE Internet Things J.*, vol. 6, no. 1, pp. 765–775, 2019.

[16] T. Zeng, G. Wang, Y. Wang, Z. Zhong, and C. Tellambura, "Statistical Covariance Based Signal Detection for Ambient Backscatter Communication Systems," in *IEEE Veh. Technol. Conf.*, pp. 1–5, 2016.

[17] H. Chen, Y.-Y. Wei, H. Chen, and W.-Q. Wang, "Adaptive Detection for Multiantenna Ambient Backscatter Communications System with MFSK Modulation," *IEEE Internet Things J.*, vol. 11, no. 16, pp. 26819–26825, 2024.

[18] W. Liu, S. Shen, D. H. K. Tsang, R. K. Mallik, and R. Murch, "An Efficient Ratio Detector for Ambient Backscatter Communication," *IEEE Trans. Wireless Commun.*, vol. 23, no. 6, pp. 5908–5921, 2024.

[19] S. Zargari, C. Tellambura, and A. Maaref, "Improved Energy-Based Signal Detection for Ambient Backscatter Communications," *IEEE Trans. Veh. Technol.*, vol. 73, no. 10, pp. 14778–14793, 2024.

[20] J. Qian, F. Gao, G. Wang, and S. Jin, "Symbol Detection and Performance Analysis of the Ambient Backscatter System," in *IEEE/CIC ICCC*, pp. 1–6, 2016.

[21] Y. Hu, P. Wang, Z. Lin, M. Ding, and Y.-C. Liang, "Machine Learning Based Signal Detection for Ambient Backscatter Communications," in *IEEE Int. Conf. Commun.*, pp. 1–6, 2019.

[22] X. Wang, R. Duan, H. Yigitler, E. Menta, and R. Jantti, "Machine Learning-Assisted Detection for BPSK-Modulated Ambient Backscatter Communication Systems," in *IEEE GLOBECOM*, pp. 1–6, 2019.

[23] W. Liu, S. Shen, D. H. K. Tsang, and R. Murch, "Enhancing Ambient Backscatter Communication Utilizing Coherent and Non-Coherent Space-Time Codes," *IEEE Trans. Wireless Commun.*, vol. 20, no. 10, pp. 6884–6897, 2021.

[24] J. Yang, L. Wang, and X. Yang, "Generalized Quadrature Space-Time Modulation for Ambient Backscatter Communication," *IEEE Wireless Commun. Lett.*, vol. 13, no. 8, pp. 2165–2169, 2024.

[25] J. Wang, P. Ren, D. Xu, and L. Lu, "A Novel Signal Detection Method Based on Multivariate Test Statistics for Ambient Backscatter Communications," in *IEEE/CIC ICCC*, pp. 713–718, 2022.

[26] A. Jha, V. Desai, and A. Patel, "Optimal Detector with Correlated RF Source Signal in Ambient Backscatter Communication Systems," in *Eur. Conf. Netw. Commun. 6G Summit*, pp. 589–594, 2025.

[27] S. Liu, S. Kar, M. Fardad, and P. K. Varshney, "Optimized Sensor Collaboration for Estimation of Temporally Correlated Parameters," *IEEE Trans. Signal Process.*, vol. 64, no. 24, pp. 6613–6626, 2016.

[28] A. Jha and A. Patel, "Detection at Multi-Antenna Reader with Correlated RF Source in Ambient Backscatter Communication," in *IEEE Int. Conf. Adv. Netw. Telecommun. Syst.*, pp. 1–3, 2024.

[29] Y. Dong, Z. Chen, J. Wang, and B. Shim, "Optimal Power Control for Transmitting Correlated Sources with Energy Harvesting Constraints," *IEEE Trans. Wireless Commun.*, vol. 17, no. 1, pp. 461–476, 2018.

[30] S. M. Kay, *Fundamentals of Statistical Signal Processing: Detection Theory*, vol. 2. Upper Saddle River, NJ: Prentice Hall, 1998.